Nat. Hazards Earth Syst. Sci. Discuss., 3, 7411–7456, 2015
www.nat-hazards-earth-syst-sci-discuss.net/3/7411/2015/
doi:10.5194/nhessd-3-7411-2015

Natural Hazards and Earth System Sciences
Discussions
Open Access
EGU

Ensemble flood forecasting to support dam water release operation using 10 and 2 km-resolution JMA Nonhydrostatic Model ensemble rainfalls

K. Kobayashi[1], S. Otsuka[2], Apip[3], and K. Saito[4]

[1]Research Center for Urban Safety and Security, Kobe University, Japan
[2]RIKEN Advanced Institute for Computational Science, Japan
[3]Research Centre for Limnology, Indonesian Institute of Sciences (LIPI), Indonesia
[4]Indonesia Forecast Research Department, Meteorological Research Institute, Japan

Received: 1 October 2015 – Accepted: 24 November 2015 – Published: 18 December 2015

Correspondence to: K. Kobayashi (kkobayashi@phoenix.kobe-u.ac.jp)

Published by Copernicus Publications on behalf of the European Geosciences Union.

Abstract

This paper presents a study on short-term ensemble flood forecasting specifically for small dam catchments in Japan. Numerical ensemble simulations of rainfall from the Japan Meteorological Agency Nonhydrostatic Model are used as the input data to a rainfall–runoff model for predicting river discharge into a dam. The ensemble weather simulations use a conventional 10 km and a high-resolution 2 km spatial resolution. A distributed rainfall–runoff model is constructed for the Kasahori dam catchment (approx. 70 km^2) and applied with the ensemble rainfalls. The results show that the hourly maximum and cumulative catchment-average rainfalls of the 2 km-resolution JMA-NHM ensemble simulation are more appropriate than the 10 km-resolution rainfalls. All the simulated inflows based on the 2 and 10 km rainfalls become larger than the flood discharge of 140 $m^3 s^{-1}$; a threshold value for flood control. The inflows with the 10 km-resolution ensemble rainfall are all considerably smaller than the observations, while, at least one simulated discharge out of 11 ensemble members with the 2 km-resolution rainfalls reproduces the first peak of the inflow at the Kasahori dam with similar amplitude to observations, although there are spatiotemporal lags between simulation and observation. To take positional lags into account of the ensemble discharge simulation, the rainfall distribution in each ensemble member is shifted so that the catchment-averaged cumulative rainfall of the Kasahori dam maximizes. The runoff simulation with the position-shifted rainfalls show much better results than the original ensemble discharge simulations.

1 Introduction

Currently, short-term ensemble flood forecasting based on ensemble numerical weather predictions (NWPs) is gaining more attention in Japan, as evidenced by the commencement of a project for ensemble weather/flood forecasting using the new K computer in Kobe, Japan (Saito, 2013b). Here, short-term flood forecasting means

NHESSD
3, 7411–7456, 2015

flood forecasts with lead times of half to one day. Cloke and Pappenberger (2009) presented a comprehensive review of medium range (2–15 days ahead) ensemble flood forecasts; however, the review focused mainly on European weather/flood forecasting examples using global ensemble predictions.

Precipitation data from NWPs are usually not considered as primary data for flood forecasting because of their accuracy, especially in the disaster prevention purpose. In Japan, primary data are obtained using radar observations of precipitation calibrated by the Japan Meteorological Agency (JMA) AMeDAS (Automated Meteorological Data Acquisition System) surface rain gauges (Makihara, 2000) or by the rain gauges of the Ministry of Land, Infrastructure, Transport and Tourism (MLIT, 2012a). It should be noted that in Japan, NWP-based weather forecasting has shown success in predicting synoptic (spatial scale of O (1000 km)) weather systems and associated precipitation events. The difference between weather and flood forecasting arises because Japanese river basins are often too small for NWP models to provide accurate estimations. The largest catchment in Japan is the Tonegawa river catchment, which is around 17 000 km^2, whereas many dam catchments are just several 100 km^2 or less. Thus, the areas of concern for most river/dam administrators are too small for global NWP models.

In the aforementioned project (Saito, 2013b), the Meteorological Research Institute tested ensemble NWPs with 2 km resolution, finer than used previously for mesoscale ensemble forecasts (e.g., Saito et al., 2010, 2011). With such a resolution, complex topographies and mesoscale convective systems can be better represented. In addition, the atmospheric model does not apply cumulus convective parameterizations, which enables us to reproduce rainfall with more realistic intensities. Therefore, such high-resolution cloud-resolving ensemble weather simulations can produce probabilistic information of intense rainfall systems better than mesoscale models with lower resolutions (Duc et al., 2013). Using ensemble rainfall forecasts produced by the JMA Nonhydrostatic Model (JMA-NHM), the authors have performed a study on the ensem-

NHESSD
3, 7411–7456, 2015

ble flood forecasting for a real extreme flood event in Niigata, Japan, using a rainfall–runoff model, the results of which are presented in this paper.

Flood disasters occurred on 27–30 July 2011 in Niigata and Fukushima prefectures, Japan, following a severe rainstorm, characterized by two rainfall peaks. According to a report by the Niigata Prefecture (Niigata, 2011), the cumulative rainfall from the onset of the rainfall until 13:00 JST on 30 July 2011 reached 985 mm at the Kasahori Dam Observatory. The cumulative rainfall at 68 rainfall observatories managed by MLIT, JMA, and Niigata Prefecture exceeded 250 mm. During this time, JMA announced "record-setting short-term heavy rainfall information" on 30 occasions. The hourly rainfall recorded from 20:00–21:00 JST on 29 July at the Tokamachi-Shinko Observatory reached 120 mm, which is an example of extreme record-setting rainfall within the region. Among the many local record-setting-rainfall amounts, this paper focuses on the Kasahori dam catchment, which is a small sub-catchment of the Shinanogawa river catchment.

The report by the Japan Weather Association (hereinafter JWA, 2011) indicates that the discharge forecasting system, operated at the Kasahori dam using short-term and very-short-term rainfall prediction by a weather model, was effective for deciding the quantity of water release from the Kasahori dam. According to the report, at 03:00 JST 29 July 2011, the discharge forecasting system predicted dam inflow of 846 $m^3 s^{-1}$ at 13:00 JST 29 July, in consideration of the observed inflow of 843 $m^3 s^{-1}$. This information, together with a telephone consultation between the JWA and dam administrator, supported the decision for the preliminary dam release. Although this clearly demonstrates the usefulness of precipitation forecasts in dam control, it is not easy to produce an accurate deterministic forecast of precipitation for a small-scale dam catchment. Therefore, this paper studies the effectiveness of ensemble flood forecasting on the Kasahori dam catchment.

The structure of this paper is as follows. The next (second) section describes additional details regarding the 2011 Niigata–Fukushima heavy rainfall using a surface weather map. The third chapter briefly describes the Kasahori dam catchment. The

NHESSD
3, 7411–7456, 2015

fourth section addresses the rainfall analysis using rain gauge and radar-derived rainfalls. The fifth section introduces the concept of the rainfall–runoff model applied in this study. The sixth section presents the results of the rainfall–runoff simulations using radar and rain gauge rainfalls for model validation. The seventh section explains about mesoscale ensemble prediction, describing ensemble weather simulation in the mesoscale and its significance before focusing on the small dam scale. The eighth section presents the results of the ensemble flood simulations for the small dam scale. The ninth section shows an additional experiment to take into account the position error of the simulated convective systems. In the final section, the concluding remarks and aspects of future work are given.

2 The 2011 Niigata–Fukushima heavy rainfall

A local heavy rainfall event occurred in July 2011 over Niigata and Fukushima prefectures, northern central Japan. Record-breaking torrential rainfall of more than 600 mm was observed during three days from 27 to 30 July, which caused severe damages in the prefectures of Niigata and Fukushima. Six people were killed and more than 13 000 houses damaged by dike breaks, river flooding, and landslides.

Figure 1 (left) indicates a surface weather map at 09:00 JST (00:00 UTC), 29 July 2011. A distinct synoptic-scale stationary front runs from the northwest to the southeast over northern central Japan. The right panel of Fig. 1 shows the three-hour accumulated rainfall from 12:00–15:00 JST (Radar–rain-gauge precipitation analysis of the Japan Meteorological Agency). Torrential rain exceeding 100 mm per 3 h occurred over the small area along the stationary front. A detailed description of this rainfall event has been published by the JMA as a special issue of the JMA Technical Report (JMA, 2013a).

NHESSD
3, 7411–7456, 2015

3 Kasahori dam catchment

Figure 2 (left) shows the Shinanogawa and Aganogawa river catchments, Japan, and Fig. 2 (right) shows an enlarged view of the Kasahori and Otani dam catchments. These catchment data were obtained from the Digital National Land Information (hereinafter DNLI) of MLIT (MLIT, 2012b). The Kasahori dam catchment area is calculated as 72.7 km^2 from the DNLI; thus, the catchment is very small. The land use of the Kasahori dam catchment is shown in Fig. 3 (left), which reveals that most of the area is occupied by forest. Therefore, the model area is treated as entirely forested in the following modelling.

4 Analysis of rainfall over the Kasahori dam catchment

The analysis of the rainfall over the Kasahori dam catchment is performed in this section. The rain gauge (RG) rainfall, JMA Radar-Composite (RC) and JMA Radar–Raingauge (RR) analysed data are used for the investigation. The descriptions of the RC and RR data are as follows:

4.1 The 1 km-resolution RC data

The echo intensity, which can be converted to rainfall intensity, is observed by 20 meteorological radar stations of the JMA and is available with 10 min temporal resolution.

4.2 The 1 km-resolution RR analysed precipitation data

The rainfall intensity observed by the radar is corrected using rain gauge data (ground observation data) and it is available with 30 min temporal resolution.

See Nagata (2011) for the further details of the analysis data. Several previous studies have been published (e.g., Kamiguchi et al., 2010; Sasaki et al., 2008) using these precipitation analysis data.

NHESSD
3, 7411–7456, 2015

4.3 RG rainfall data

The time-series data of hourly rainfall of the Otani dam, Otani, Koumyozan, Kasahori dam, Kasahori, and Dounokubo rainfall observatories, shown in Fig. 3 (right), are used as the ground observation data. A Thiessen polygon is drawn based on the locations of the observatories, by which each observatory is assigned a representative area. Then, the hourly rainfall data are given to each representative area in the calculation. The cumulative and maximum rainfalls for the period 01:00 JST 28 July to 24:00 JST 30 July were: 955 and 83 mm at the Kasahori dam, 722 and 71 mm at Kasahori, 786 and 74 mm at Koumyozan, and 723 and 78 mm at Dounokubo, respectively.

The catchment-averaged rainfalls are calculated using these three types of rainfall data (RC, RR, and RG) and shown in Fig. 4. From the figure, it can be seen that the catchment-average rainfalls of the RG and RR are similar, whereas the RC is smaller than the other two. The cathment-avearaged cumulative rainfall during the period, based on the RG, RR, and RC, reaches 765.0, 762.8, and 568.5 mm, respectively. In other words, the cumulative rainfall by the RC is 0.74 times that of the ground observation, whereas the value by the RR is almost similar to the RG. Figure 5 shows the spatial distributions of the cumulative rainfall for the 2011 rainfall event around the Shinanogawa and Aganogawa river catchment by RC and RR (left and right panels, respectively), while Fig. 6 shows those of the Kasahori dam catchment. It is apparent from Fig. 5 that the distributions by RC and RR show similar patterns in the mesoscale. However, it becomes slightly different when focusing on the small-scale Kasahori dam catchment, as shown in Fig. 6. To verify whether the RC precipitation in this region is always smaller than RR, Figs. 7 and 8 show the rainfall patterns for another rainfall event in 2004, when flooding also occurred in the region. The damage by the flooding due to the 2004 event was even greater than that caused by the 2011 rainfall, although the total amount of rainfall in 2011 was larger. Figures 7 and 8 show that the RC rainfall is larger than RR rainfall for the 2004 rainfall. The RR rainfall is obtained by correcting the RC using RG rainfall. Thus, the magnitude of the relation between the RC and

NHESSD
3, 7411–7456, 2015

RR rainfalls depends on the magnitude of the RG rainfall compared with the RC. The precipitation by RC is occasionally larger than the RR rainfall when the RG rainfall is smaller than RC and sometimes, vice versa. As the RC can be obtained at 10 min interval with greater spatial coverage, it is considered more reasonable for use in future real-time operational purposes, though the authors do not carry out the operation. Thus, the calibration of the rainfall–runoff model is performed using RC rainfall.

5 Distributed Rainfall–Runoff (DRR) model

The exclusive purpose of the paper is to investigate the usefulness of 2 km NHM rainfall which is relatively novel in the meteorological field. Thus, a distributed rainfall–runoff (hereinafter DRR) model whose usefulness is already validated on some level was applied to the Kasahori dam catchment. The DRR model applied is that originally developed by Kojima and Takara (2003) called CDRMV3. The details of this DRR model can be seen in the work by Apip et al. (2011). In the DRR model, the surface and river flows are simulated using a 1-D kinematic wave model. The subsurface flow is simulated using a q–h relationship developed by Tachikawa et al. (2004). The schematic of the q–h relationship is shown in Fig. 9, where q is the discharge per unit width and h is the water depth, as shown in Fig. 9a. The mathematical expression is as follows:

$$q(h) = \begin{cases} v_m d_m \left(\frac{h}{d_m}\right)^{\beta}, & (0 \le h \le d_m) \\ v_m d_m + v_a (h - d_m), & (d_m < h \le d_a) \\ v_m d_m + v_a (h - d_m) + \alpha (h - d_a)^m, & m = \frac{5}{3}, (d_a < h) \end{cases} \quad (1)$$

where $v_m = k_m i$, $v_a = k_a i$, $\alpha = \sqrt{i / N_{slope}}$ and D is the thickness of the layer, shown in Fig. 9a; $d_a - d_m$ is the area of the saturated flow; d_m is the area of unsaturated flow; v_m is the unsaturated flow velocity; k_m is the hydraulic conductivity in d_m; i represents the slope gradient; v_a is the saturated flow velocity; k_a is the hydraulic conductivity in

NHESSD
3, 7411–7456, 2015

$d_a - d_m$; and N_{slope} represents the equivalent roughness coefficient of the slope. $\beta k_m = k_a$ needs to be satisfied to establish the continuity of the q–h relationship. As mentioned in the previous section, the parameters of the DRR model are identified using the RC. The equivalent roughness coefficient of the forest, the Manning coefficient of the river, and identified soil-related parameters are described in Table 1.

6 Results of the rainfall–runoff simulation with radar and rain gauge rainfalls

The inflow to the Kasahori dam is simulated using the DRR model. The RG, RC, and RR data are used as the inputs to the runoff simulations. The three hydrographs with the parameters identified by the RC are shown in Fig. 10. The simulated hydrograph with the RC rainfall is in relatively good agreement with the observations, which is to be expected because the model parameters are calibrated against the RC rainfall. The cumulated catchment-averaged rainfall of the RC for the period is 568.5 mm, while the total discharge becomes 577.0 mm if we use $r = 3.6Q/A$ where r is the rainfall, Q the discharge and A the catchment area; thus even the initially saturated water in the catchment is slightly drained in the simulation. The simulated hydrographs for the other two rainfalls are larger than the observations. We do not address the magnitude of the relationship in this paper because it is not possible to determine more accurate rainfall data. The RG, RC, and RR measurements all have strengths and weaknesses; however, we focus on the consideration of RC for use because of the frequency of the data, i.e. 10 min interval.

7 Mesoscale ensemble prediction

Two 11-member ensemble forecasts with different horizontal resolutions (10 and 2 km) were conducted for the 2011 Niigata–Fukushima heavy rainfall event using the JMA-NHM (Saito et al., 2006; Saito, 2012) as the forecast model. The 10 km ensemble prediction system (EPS) uses the JMA's operational mesoscale 4D-VAR analysis of

NHESSD
3, 7411–7456, 2015

12:00 UTC 28 July and the JMA's global spectral model (GSM) forecast from the same time as the initial and boundary conditions of the control run. As for the initial and lateral boundary conditions, perturbations from the JMA's one-week global ensemble prediction from 12:00 UTC 28 July were employed, whose detailed procedures are given in Saito et al. (2010, 2011). The 2 km EPS is a downscaling of the 10 km EPS with a 6 h time lag, using the forecasts of the 10 km EPS as the initial and boundary conditions (Fig. 11).

The bulk method that predicts the mixing ratios of six water species (water vapour, cloud water, rainwater, cloud ice, snow, and graupel) and the number density of cloud ice was adopted as the cloud microphysical process. The 10 km EPS applied the modified Kain–Fritsch convective parameterization scheme, while the 2 km EPS did not use convective parameterization. Other physical processes of the two systems were almost the same to those of the operational mesoscale model and the local forecast model (LFM) of JMA (JMA, 2013b). The verification of the statistical performance of similar double-nested EPSs have been given by Duc et al. (2013).

Figure 12 (left) shows the three-hour accumulated rainfall from 12:00–15:00 JST by the control run of the 10 km EPS. Although the maximum value of the predicted rainfall (74 mm) is somewhat weaker than the observation (right panel of Fig. 1), the region of intense rainfall is simulated well. The right panel of Fig. 12 indicates the forecast by each member of the 10 km EPS. Seemingly, the result of each ensemble member resembles the others, and the basic characteristic features of the observed rainfall are simulated well. The maximum rainfall was obtained by member p02 (89 mm). A common feature seen in these figures is that weak fake rainfall appears over the coastal region facing the Sea of Japan, which is likely produced by the Kain–Fritsch convective parameterization.

Figure 13 shows the corresponding results by the 2 km EPS. The concentration of intense precipitation is produced more clearly; the maximum rainfall of which reaches 237 mm. The areas of weak rainfall over the west coastal region, appeared in Fig. 12, no longer develop because of the removal of the convective parameterization. A de-

NHESSD
3, 7411–7456, 2015

tailed analysis of the two EPSs (ensemble spread and fraction skill scores) and the result of a sensitivity experiment to the orography have been presented by Saito et al. (2013).

8 Ensemble flood simulation

Using the ensemble rainfalls from the JMA-NHM, explained in the previous section, the ensemble flood simulation focusing on the Kasahori dam catchment was performed. A flowchart is shown in Fig. 14 to explain briefly again the overall procedure of the methodology for the ensemble simulations used in the paper.

The catchment-averaged ensemble rainfalls obtained from the 10 and 2 km-resolution NHM are shown in Figs. 15 and 16, respectively. Figure 15 (upper) shows the control run and five negatively perturbed members: m01–m05 (m indicates minus), and Fig. 15 (lower) presents the control run and five positively perturbed members: p01–p05 (p indicates positive).

It is apparent from the figures that the magnitude of the 10 km-resolution ensemble rainfall is basically lower than the RC rainfall. Thus, the dam inflows, obtained from the RC parameters in Table 1 with the 10 km-resolution ensemble rainfall, lead to lower magnitude discharge compared with the ground observations (shown later in the paper).

Figure 16 (upper) shows the control run and members m01–m05, and Fig. 16 (lower) presents the control run and members p01–p05 for the 2 km-resolution NHM. The figures reveal that the first peak in the 2 and 10 km-resolution ensemble simulations appears 2–4 h earlier than that in the observation. The magnitudes of some 2 km-resolution ensemble rainfalls are equivalent to that of the RC rainfall. Thus, dam inflows using the RC parameters in Table 1 with the 2 km-resolution ensemble rainfall can indicate discharge with equivalent magnitude (shown later in the paper). Figure 17 shows the spatial patterns of the cumulative ensemble rainfalls from 03:00 JST 29 July 2011 to 03:00 JST 30 July 2011 by the 11 ensemble simulations (upper: 10 km resolution;

NHESSD
3, 7411–7456, 2015

lower: 2 km resolution). The figures indicate that the 2 km-resolution NHM rainfalls are apparently larger than the 10 km-resolution rainfalls. Tables 2 and 3 show the cumulative and maximum hourly rainfalls from the 10 and 2 km-resolution NHMs, respectively, averaged over the Kasahori dam catchment, which show that the 10 km-resolution rainfalls are smaller than the 2 km-resolution rainfalls. The maximum cumulative rainfall of the 2 km-resolution NHM is realised in p02: 175.5 mm. Table 2 also shows the average cumulative rainfalls of both the 10 and 2 km-resolution NHMs. The average cumulative rainfall in the 2 km-resolution NHM is greater than in the 10 km-resolution NHM. With regard to the maximum hourly rainfall in Table 3, p02 shows the highest values in both the 10 and 2 km-resolution NHMs. The maximum hourly rainfall in the 2 km-resolution NHM is also greater than that in the 10 km-resolution NHM. This tendency is also true in the average maximum hourly rainfall shown in Table 3.

The simulation results of dam inflow are shown in Figs. 18 and 19. Figure 18 (upper) shows the simulated inflow to the Kasahori dam with the control run and negatively perturbed rainfalls of the 10 km-resolution NHM. Figure 18 (lower) presents the inflow with the control run and positively perturbed rainfalls of the 10 km-resolution NHM. Figure 18 shows that all the inflows to the Kasahori dam are lower than the observations; however, these inflows are more than the flood discharge of 140 $m^3 s^{-1}$, which is the threshold quantity for flood control operation.

Figure 19 shows the simulated discharge with the 2 km-resolution ensemble rainfalls. Figure 19 (lower) shows that at least the first peak of the dam inflow in p02 shows a comparable value with that of the observed inflow; the peak discharge of the observation is 843 $m^3 s^{-1}$, whereas it is 779 $m^3 s^{-1}$ with the p02 of the 2 km-resolution NHM. However, the occurrence of the first peak in the simulation is four hours earlier than indicated by the observations. The fact that one of the ensemble flood discharges with the 2 km-resolution NHM shows approximately equivalent magnitude of discharge with the observed first peak discharge, despite the forward shift in occurrence time, implies that the ensemble flood prediction with the 2 km-resolution NHM could potentially be used as a reference in dam operations, although the discharge reproduction

NHESSD
3, 7411–7456, 2015

is still not fully satisfactory both in quality and quantity. The ensemble flood simulations with the 10 km-resolution NHM could not reproduce the peak at all. Moreover, the first peak of the simulated inflow with the control run of the 2 km-resolution NHM attains only 614 $m^3 s^{-1}$. A single value from a deterministic (i.e., control run only) NWP (i.e., prevailing prediction) might fail to capture a realistic discharge, whereas ensemble simulations produce additional prediction ranges that cover the higher observed discharge values.

In the actual operation of the Kasahori dam, the decision related to water release for flood control is based on a flood discharge of 140 $m^3 s^{-1}$. The dam inflows from the control run and the other 10 ensemble rainfall predictions of both the 2 and 10 km-resolution NHMs, all predict that the dam inflow is above the flood discharge threshold. The single weather simulation produces solely a deterministic value, which does not reflect the uncertainty of the initial conditions, whereas ensemble simulations enhance confidence in the prediction by incorporating the uncertainty. The exceedance probability of 11/11 by the ensemble simulations is numerically the same as the probability of 1/1 by a single simulation. However, the physical implications of these two values are different in terms of confidence and significance.

All the dam inflow simulations, however, show that the second and third peaks of the inflow are much smaller than indicated by the observations. In the actual flood event, the so-called "Tadashigaki operation (emergency operation)" was implemented at around the time of the second and third peaks. In the Tadashigaki operation, the dam outflow has to equal the inflow to avoid dam failure as the water level approaches overtopping of the dam body. The runoff simulations did not reproduce such a critical situation this time because the second and third discharge peaks are not properly reproduced. This is a deficiency of the ensemble forecast method at this time. The accumulated inflow volume to the dam of both the observation and 2 km ensemble simulation from 03:00 JST 29 July 2011 to 03:00 JST 30 July 2011 is shown in Fig. 20. It can be seen that the inflow volumes are somehow comparable with the observations until the 1st peak is observed, though the discrepancy becomes larger afterwards. This

NHESSD
3, 7411–7456, 2015

will cause critical hardship for dam operation if the ensemble flood prediction were used in isolation, especially after the 1st peak.

9 Position shift of ensemble rainfalls

Numerical weather prediction have inevitable forecast errors. The current case has large amount of accumulated rainfall within a limited area, and is sensitive to the position error. Although ensemble simulation represents the uncertainty to some extent, the ensemble spread tends to under-dispersive because of imperfect model/initial condition representations and limited ensemble sizes. Duc et al. (2013) verified the spatial–temporal Fractions Skill Score (FSS) of 10 km/2 km ensemble forecasts for heavy rainfall events occurring over central Japan from 3 July 2010 to 2 August 2010. They showed that a spatial scale of 60 km (positional lag of 30 km) should be considered to obtain a reasonable reliability from a high-resolution ensemble forecast. Thus, it is important to take into account the position error within a reasonable distance before input to the runoff model.

To improve the ensemble rainfalls in quantity and timing, the cumulative rainfalls of each ensemble member are calculated and the rain distribution is translated within 30 km from the original position so that the catchment-averaged cumulative rainfall for the Kasahori dam maximizes. The analysis is carried out using the 2 km resolution, 30 h rainfall after the simulation. This position change corresponds to consideration of a 30 km positional lag to detect a risk of the maximum rainfall amount. Figure 21 shows the examples of the positon shifts for cntl, m02, p03 and p04. Although the ensemble forecasts produce high cumulative rainfall, the original peak lies to the south of the Kasahori dam in all four members shown in Fig. 21. Figure 22 shows the spatial distribution of the position-shifted cumulative ensemble rainfalls with the 2 km resolution. Comparing Figs. 17 and 22, it is apparent that the rainfall intensity becomes higher. The simulated discharges with these position-shifted rainfalls are shown in Fig. 23. Figure 23 indicates that the 1st peak discharge simulated becomes high enough com-

NHESSD
3, 7411–7456, 2015

pared with the observed discharge. Timing of the first peak is also improved, and particularly, some members reproduce the exact timing. Figure 23 shows the ensemble mean of the discharge as well since the ensemble mean becomes more informative compared to that in the experiment without position shifting. Figure 24 shows the inflow volume into the reservoir based on the observation and position-shifted ensemble simulations; the simulated inflow volume becomes comparable to the observed inflow volume. These results indicate that the ensemble rainfall simulation with position shift brings better performance although testing with more cases is desirable to confirm that.

As indicated in the section on mesoscale ensemble prediction, it is known that ensemble weather simulations can be useful in adding value to weather forecasts. In the current operational weather forecasting, it is not necessarily expected that the weather will be predicted accurately for any specific location. However, accurate prediction over dam catchments is the main concern of river dam administrators. In this regard, this paper shows clearly that although the original 2 km prediction forecast provides much better results than that with the 10 km-resolution prediction, greater accuracy is still desirable. For example, in dam/reservoir operations, the reliable prediction of the peak timing, flood duration, and runoff volume are extremely important parameters necessary to avoid erroneous operation. The results with original ensemble rainfalls here do not match the current requirements; however, the position-shifted 2 km-resolution ensemble rainfall could be a useful tool for supporting operational decisions after statistical validation with various rainfall events, which would not be possible based on previous simulations with coarser resolutions.

10 Concluding remarks and future aspects

This paper presents an example of short-term (lead times of less than a day) ensemble flood forecasting for a typical small-scale dam catchment in Japan. The Kasahori dam catchment (approx. 70 km^2) in Niigata, Japan, was selected as the study site. Japanese river catchments tend to be small and thus, floods in such catchments are

NHESSD
3, 7411–7456, 2015

often in the category of flash flood of continental rivers. In other words, the rainfall over the small catchments and associated flood processes are too rapid to be captured well by coarse-resolution NWP models. Thus, the JMA-NHM with 2 km resolution was used to simulate the rainfall over the catchment. As the result, all 11 × 2 ensemble simulations (i.e. 10 and 2 km resolutions) predicted that the dam inflow would exceed the flood discharge of 140 $m^3 s^{-1}$, which is the threshold quantity for flood control. However, only one out of 11 × 2 (2 and 10 km resolutions) ensemble predicted discharges, based on the ensemble rainfalls, reproduced in a broad sense the first peak of the observed discharge of the historically rare flood that occurred on 28–30 July 2011 with a 4 h lag in the occurrence time. Nevertheless, this is considered insufficient for the dam operations. In contrast, the position-shifted ensemble flood simulations show much better results and become comparable to the observation, indicating the importance of appropriate treatment of forecast uncertainties.

In any case, overall results are considered on some level helpful for decision-making related to flood control, especially as a supporting tool in addition to discharge observations and forecasting with radars. Likewise, improving the accuracy of original rainfall forecasted by high-resolution state-of-the-art numerical models, dense observation networks, and advanced data assimilation techniques is still essential. In future work, further applications of ensemble flood forecasting for different events will be conducted to derive further generalities of ensemble flood simulations. The validity of the position shift needs to be further investigated as well.

Acknowledgements. The first author performed the field survey of the region as a member of the investigation group of the Japan Society of Civil Engineers, led by Nobuyuki Tamai at the University of Tokyo. Through these activities, we received much useful information and data from the Niigata Prefecture. The authors would like to thank Tamai and the many other people who offered their help. This study is supported by the MEXT Global COE programme, "Sustainability/Survivability Science for a Resilient Society Adaptable to Extreme Weather Conditions" (GCOE-ARS, Programme Leader: Kaoru Takara, DPRI, Kyoto University). The authors appreciate the help provided by Takara. The ensemble forecast using the JMA-NHM was conducted at the Meteorological Research Institute (MRI) as a part of the Grant-in-Aid for Scientific Re-

NHESSD
3, 7411–7456, 2015

search (21 244 074) and the Strategic Programs for Innovative Research, and we thank Seiji Origuchi and Hiromu Seko for their help in performing the ensemble forecasts.

References

Apip, R., Sayama, T., Tachikawa, Y., and Takara, K.: Spatial lumping of a distributed rainfall-sediment-runoff model and its effective lumping scale, Hydrol. Process., 26, 855–871, doi:10.1002/hyp.8300, 2011.

Cloke, H. L. and Pappenberger, F.: Ensemble flood forecasting: a review, J. Hydrol., 375, 613–626, doi:10.1016/j.jhydrol.2009.06.005, 2009.

Duc, L., Saito, K., and Seko, H.: Spatial–temporal fractions verification for high resolution ensemble forecasts, Tellus, 65, 18171, doi:10.3402/tellusa.v65i0.18171, 2013.

Japan Meteorological Agency: Report on "the 2011 Niigata-Fukushima Heavy Rainfall Event", Typhoon Talas (1112) and Typhoon Roke (1115), Tech. Rep. JMA, 134, 253 pp., available at: http://www.jma.go.jp/jma/kishou/books/gizyutu/134/ALL.pdf (last access: 22 July 2015), 2013a (in Japanese).

Japan Meteorological Agency: Outline of the Operational Numerical Weather Prediction at the Japan Meteorological Agency, available at: http://www.jma.go.jp/jma/jma-eng/jma-center/nwp/outline2013-nwp/index.htm (last access: 22 July 2015), 2013b.

Japan Weather Association: Overview of the Kasahori Dam Rainfall–Runoff Prediction System, available at: http://www.jwa.or.jp/var/plain_site/storage/original/application/08b6516f714560696bcbed8422ad99b6.pdf (last access: 22 July 2015), 2011 (in Japanese).

Kamiguchi, K., Arakawa, O., Kitoh, A., Yatagai, A., Hamada, A., and Yasutomi, N.: Development of APHRO_JP, the first Japanese high-resolution daily precipitation product for more than 100 years, Hydrol. Res. Lett., 4, 60–64, doi:10.3178/hrl.4.60, 2010.

Kojima, T. and Takara, K.: A grid-cell-based distributed flood runoff model and its performance, IAHS-AISH P., 282, 234–240, 2003.

Makihara, Y.: Algorithm for precipitation nowcasting focused on detailed analysis using radar and rain gauge data, Technical Report, MRI, 39, 63–111, 2000.

MLIT: X Band MP Radar Rainfall Information, available at: http://www.river.go.jp/xbandradar (last access: 22 July 2015), 2012a (in Japanese).

NHESSD

3, 7411–7456, 2015

MLIT: Digital National Land Information download service, available at: http://nlftp.mlit.go.jp/ksj/ (last access: 22 July 2015), 2012b (in Japanese).
Nagata, K.: Quantitative Precipitation Estimation and Quantitative Precipitation Forecasting by the Japan Meteorological Agency, RSMC Tokyo – Typhoon Center Technical Review 13, 37–50, available at: http://www.jma.go.jp/jma/jma-eng/jma-center/rsmc-hp-pub-eg/techrev/text13-2.pdf (last access: 22 July 2015), 2011 (in Japanese).
Niigata Prefecture: Niigata/Fukushima Extreme Rainfall Disaster Survey Documentation (as of 22 Aug 2011), available at: http://www.pref.niigata.lg.jp/kasenkanri/1317679266491.html, (last access: 22 July 2015), 2011 (in Japanese).
Saito, K.: The Japan Meteorological Agency nonhydrostatic model and its application to operation and research, in tech, Atmos. Model Appl., InTech, 85–110, doi:10.5772/35368, 2012.
Saito, K., Fujita, T., Yamada, Y., Ishida, J., Kumagai, Y., Aranami, K., Ohmori, S., Nagasawa, R., Kumagai, S., Muroi, C., Kato, T., Eito, H., and Yamazaki, Y.: The operational JMA Nonhydrostatic Mesoscale Model, Mon. Weather Rev., 134, 1266–1298, doi:10.1175/MWR3120.1, 2006.
Saito, K., Kuroda, T., Kunii, M., and Kohno, N.: Numerical simulations of Myanmar Cyclone Nargis and the associated storm surge, Part 2: Ensemble prediction, J. Meteorol. Soc. Jpn., 88, 547–570, doi:10.2151/jmsj.2010-316, 2010.
Saito, K., Hara, M., Kunii, M., Seko, H., and Yamaguchi, M.: Comparison of initial perturbation methods for the mesoscale ensemble prediction system of the Meteorological Research Institute for the WWRP Beijing 2008 Olympics Research and Development Project (B08RDP), Tellus A, 63, 445–467, doi:10.1111/j.1600-0870.2010.00509.x, 2011.
Saito. K., Origuchi, S., Duc, L., and Kobayashi, K.: Mesoscale ensemble forecast experiment of the 2011 Niigata-Fukushima heavy rainfall, Techical Report, JMA, 134, 170–184, available at: http://www.jma.go.jp/jma/kishou/books/gizyutu/134/ALL.pdf (last access: 22 July 2015), 2013a (in Japanese).
Saito, K., Tsuyuki, T., Seko, H., Kimura, F., Tokioka, T., Kuroda, T., Duc, L., Ito, K., Oizumi, T., Chen, G., Ito, J., and SPIRE Field 3 Mesoscale NWP group: Super high-resolution mesoscale weather prediction, J. Phys. Conf. Ser., 454, 012073, doi:10.1088/1742-6596/454/1/012073, 2013b.
Sasaki, H. and Kurihara, K.: Relationship between precipitation and elevation in the present climate reproduced by the non-hydrostatic regional climate model, SOLA, 4, 109–112, doi:10.2151/sola.2008-028, 2008.

NHESSD
3, 7411–7456, 2015

Tachikawa, Y., Nagatani, G., and Takara, K.: Development of stage–discharge relationship equation incorporating saturated/unsaturated flow mechanism, Annual J. Hydraul. Eng., JSCE, 48, 7–12, 2004.

NHESSD
3, 7411–7456, 2015

Table 1. Equivalent roughness coefficient of the forest, Manning's coefficient of the river, and soil-related parameters identified by the Radar-Composite.

Forest [$m^{-1/3}$ s]	River [$m^{-1/3}$ s]	D [m]	k_s [$m\,s^{-1}$]
0.15093	0.004	0.320	0.0005

NHESSD
3, 7411–7456, 2015

Table 2. Cumulative rainfall of 2 and 10 km-resolution ensemble rainfall simulations.

	Cntl	p01	p02	p03	p04	p05	m01	m02	m03	m04	m05	ave.
10 km	108.8	130.2	140.6	113.5	140.2	97.9	111.6	93.5	102.2	101.2	100.5	112.7
2 km	156.7	124.6	175.5	128.5	165.1	93.9	111.3	98.2	169.1	86.9	148.8	132.6

NHESSD
3, 7411–7456, 2015

Table 3. Maximum hourly rainfall of 2 and 10 km-resolution ensemble rainfall simulations.

	Cntl	p01	p02	p03	p04	p05	m01	m02	m03	m04	m05	ave.
10 km	26.8	17.6	41.7	27.9	18.7	18.2	27.5	16.0	21.9	28.9	29.4	23.5
2 km	41.4	32.4	49.5	31.8	37.0	27.6	28.8	29.8	42.5	28.2	30.8	34.5

NHESSD
3, 7411–7456, 2015

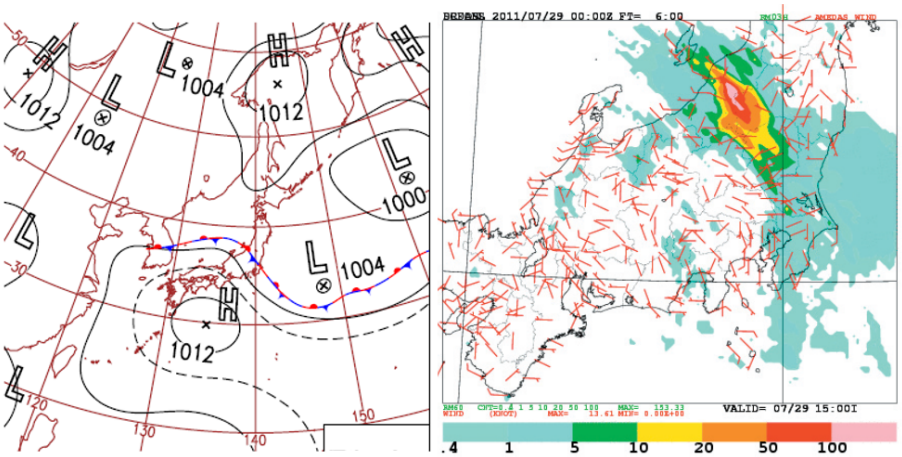

Figure 1. Surface weather map for 09:00 JST, 29 July 2011 (left). Three-hourly accumulated observed rainfall from 12:00–15:00 JST (right).

NHESSD
3, 7411–7456, 2015

Ensemble flood forecasting to support dam water release operation

K. Kobayashi et al.

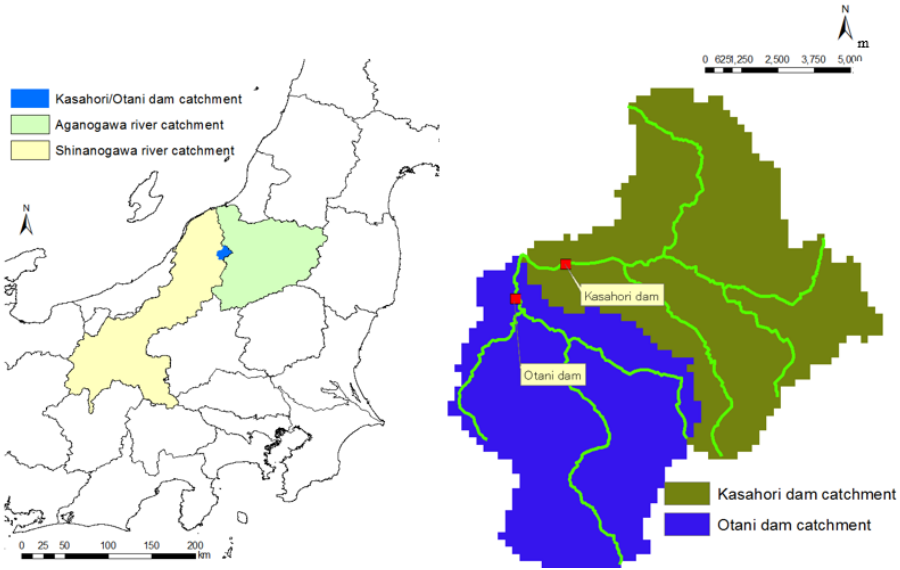

Figure 2. Shinanogawa and Aganogawa river catchments (left). Kasahori dam and Otani dam catchments (right).

NHESSD
3, 7411–7456, 2015

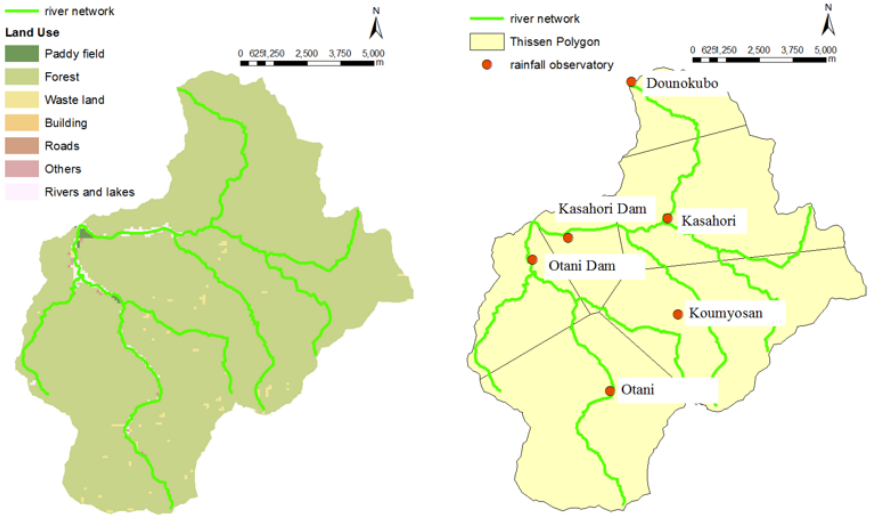

Figure 3. Land use of the Kasahori and Otani dam catchments (left). Rainfall observatories and Thiessen polygons of the Kasahori and Otani dam catchments (right).

NHESSD
3, 7411–7456, 2015

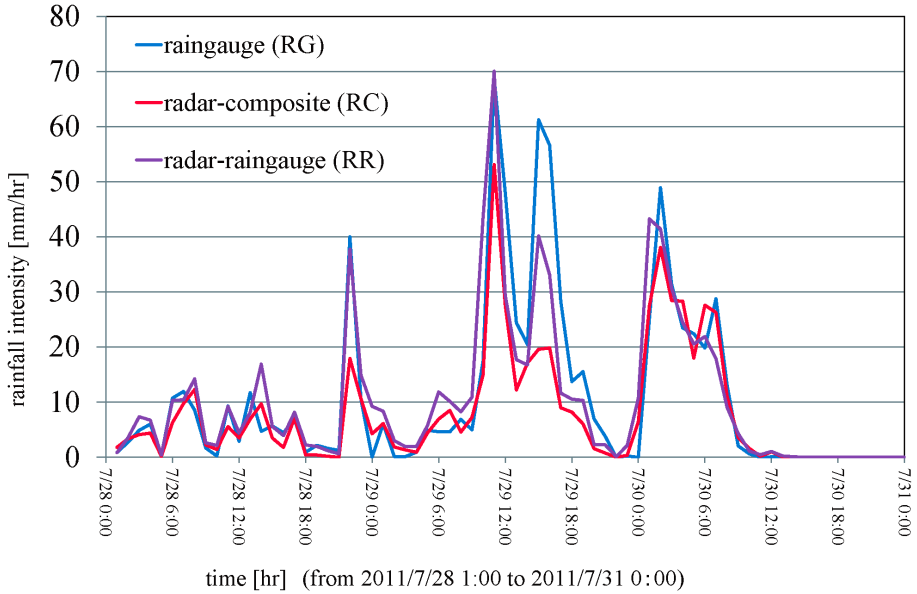

Figure 4. Catchment-averaged rainfalls of the Kasahori dam catchment.

NHESSD
3, 7411–7456, 2015

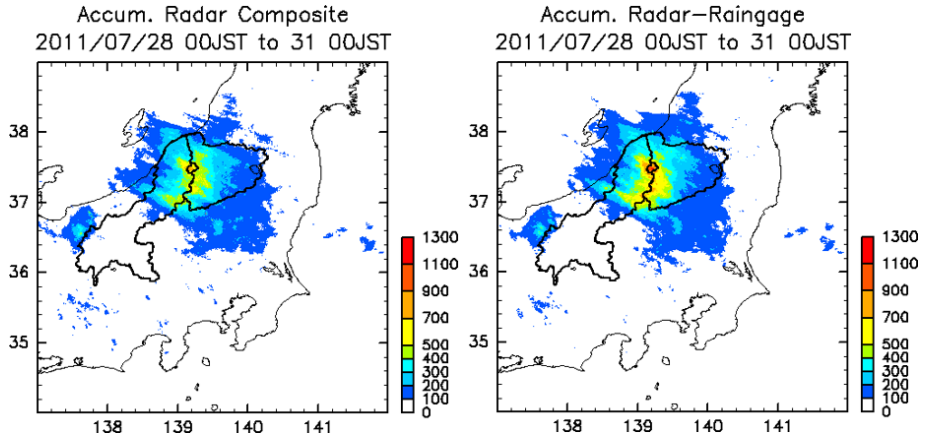

Figure 5. Spatial patterns of cumulative rainfalls around the Shinanogawa and Aganogawa catchments using Radar-Composite (left) and Radar-Raingauge (right) for the 2011 rainfall event.

NHESSD
3, 7411–7456, 2015

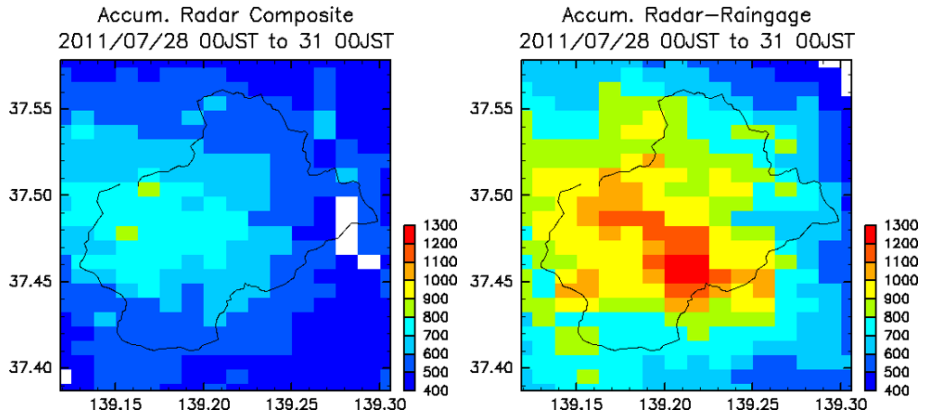

Figure 6. Spatial patterns of cumulative rainfalls around the Kasahori dam catchment using Radar-Composite (left) and Radar–Raingauge (right) for the 2011 rainfall event.

NHESSD
3, 7411–7456, 2015

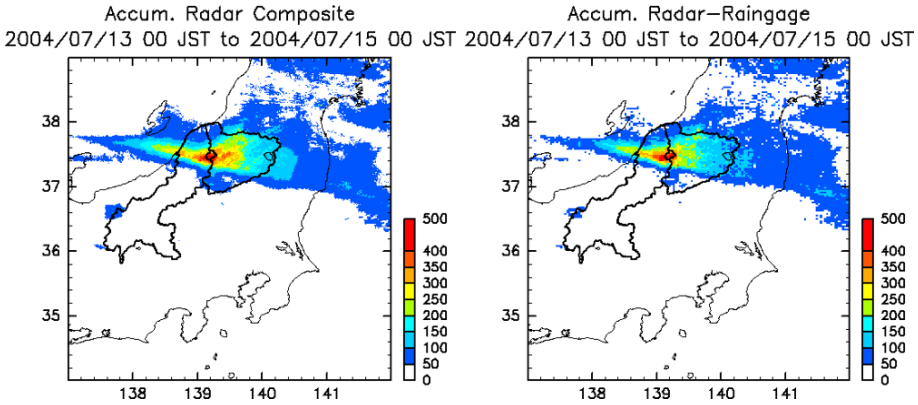

Figure 7. Spatial patterns of cumulative rainfalls around the Shinanogawa and Aganogawa catchments using Radar-Composite (left) and Radar-Raingauge (right) for the 2004 rainfall event.

NHESSD
3, 7411–7456, 2015

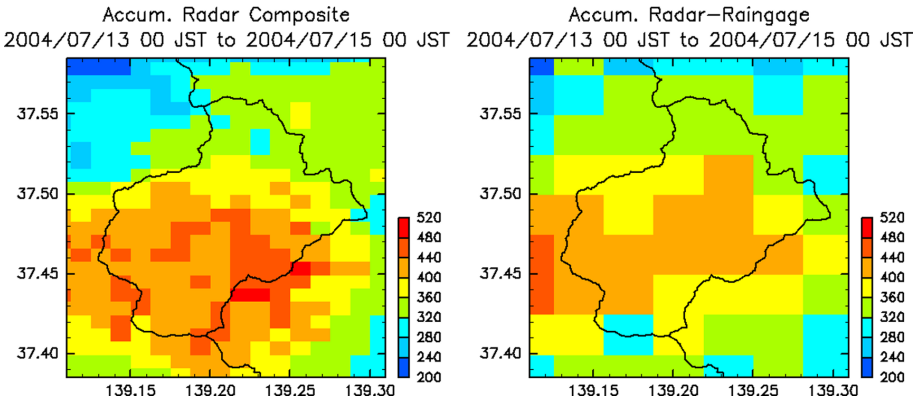

Figure 8. Spatial patterns of cumulative rainfalls around the Kasahori dam catchment using Radar-Composite (left) and Radar-Raingauge (right) for the 2004 rainfall event.

NHESSD
3, 7411–7456, 2015

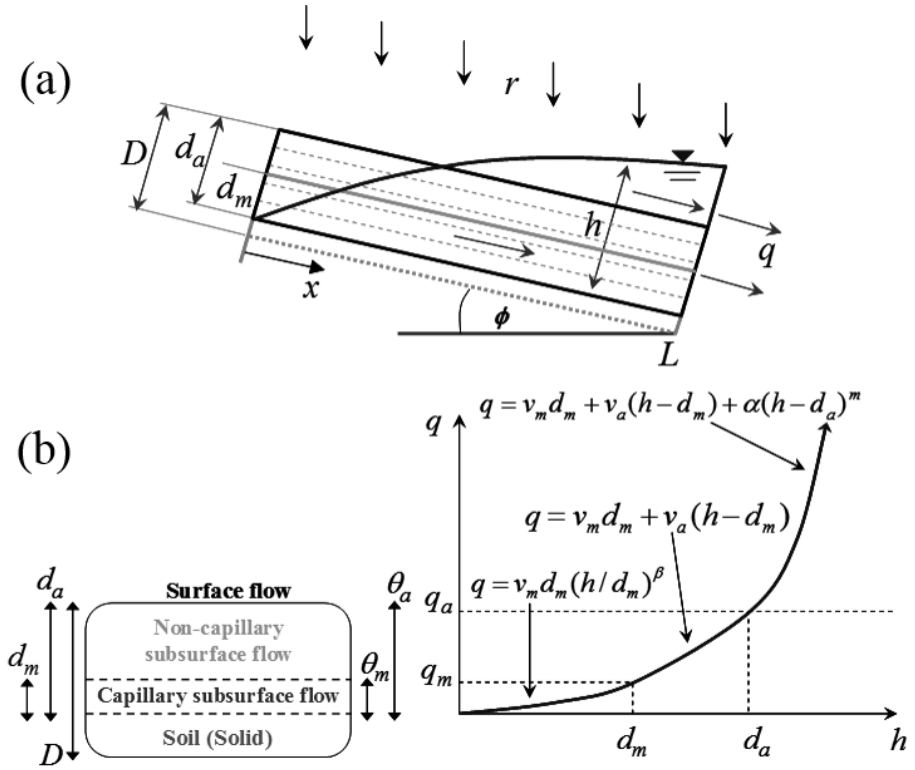

Figure 9. (a) Schematic of the surface–subsurface flow on a hillslope (upper), and **(b)** relationship between unit width discharge q and water depth h in each grid (lower).

NHESSD
3, 7411–7456, 2015

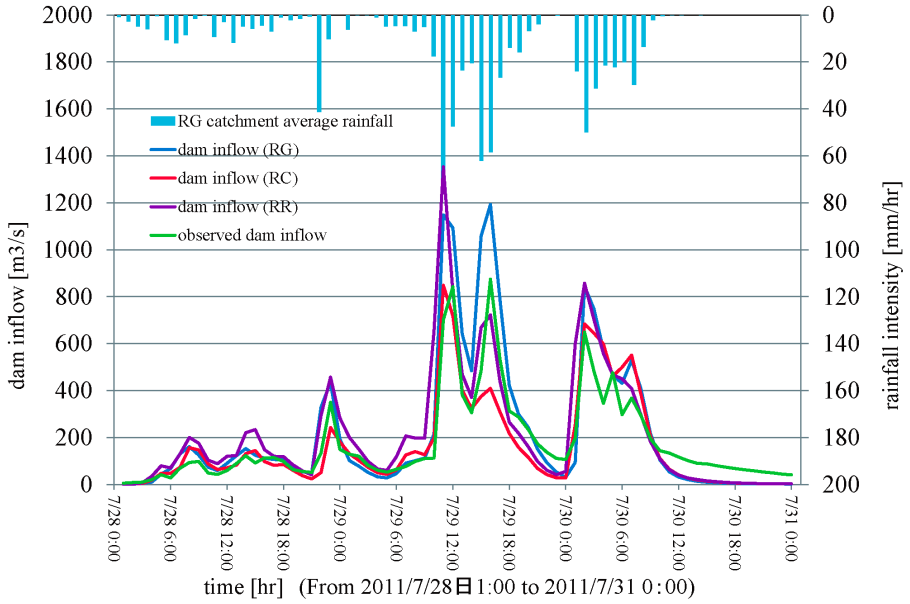

Figure 10. Dam inflows for three rainfalls using the parameters identified with Radar-Composite.

NHESSD
3, 7411–7456, 2015

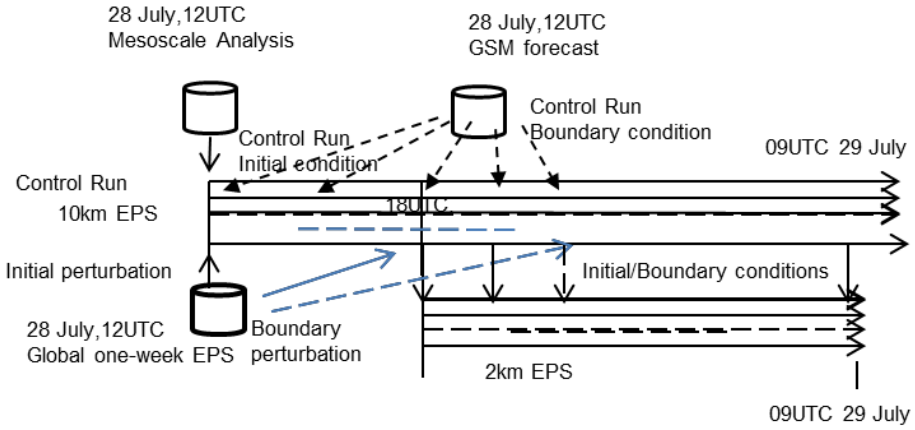

Figure 11. Schematic of the 10 km and 2 km EPSs.

NHESSD
3, 7411–7456, 2015

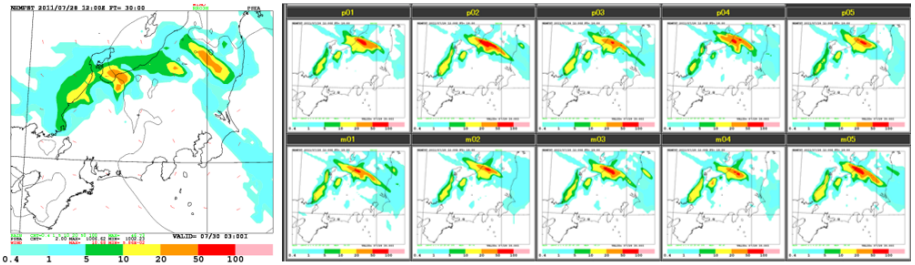

Figure 12. Three-hourly accumulated rainfall from 12:00–15:00 JST by the control run of the 10 km EPS (left). Same as in the left figure, but the forecast by each member of the 10 km EPS (right). Upper columns show results by positive perturbation members (p01–p05), while lower columns show those by negative perturbation members (m01–m05).

NHESSD
3, 7411–7456, 2015

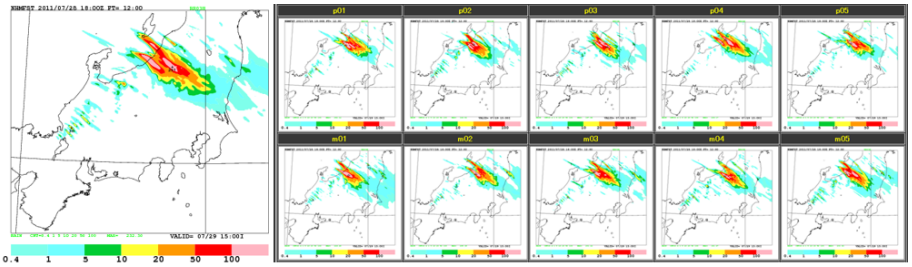

Figure 13. Same as in Fig. 12, but for forecasts by the 2 km EPS.

NHESSD
3, 7411–7456, 2015

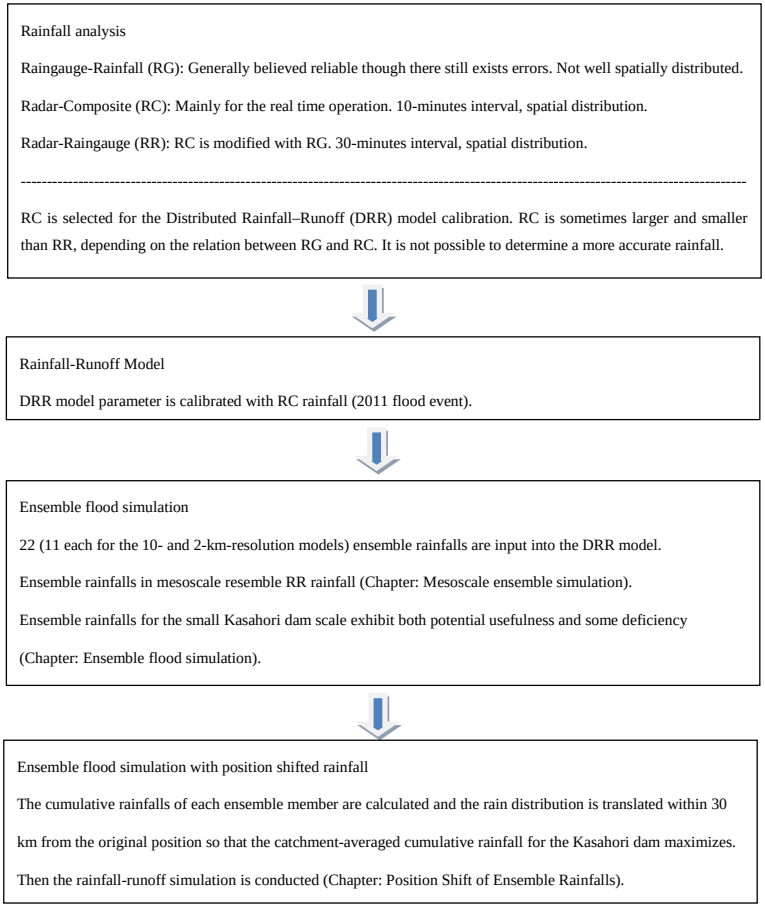

Figure 14. Flowchart of the overall procedure for the ensemble weather/flood simulation.

NHESSD
3, 7411–7456, 2015

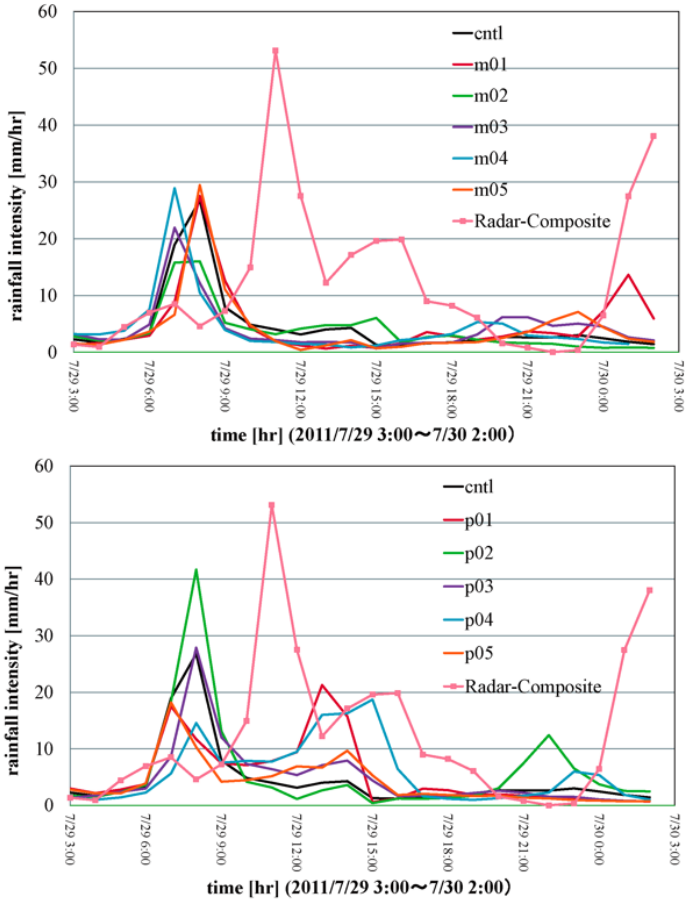

Figure 15. Catchment-averaged rainfalls with JMA-NHM 10 km-resolution ensemble simulation (upper: control run and negatively perturbed members; lower: control run and positively perturbed members).

NHESSD
3, 7411–7456, 2015

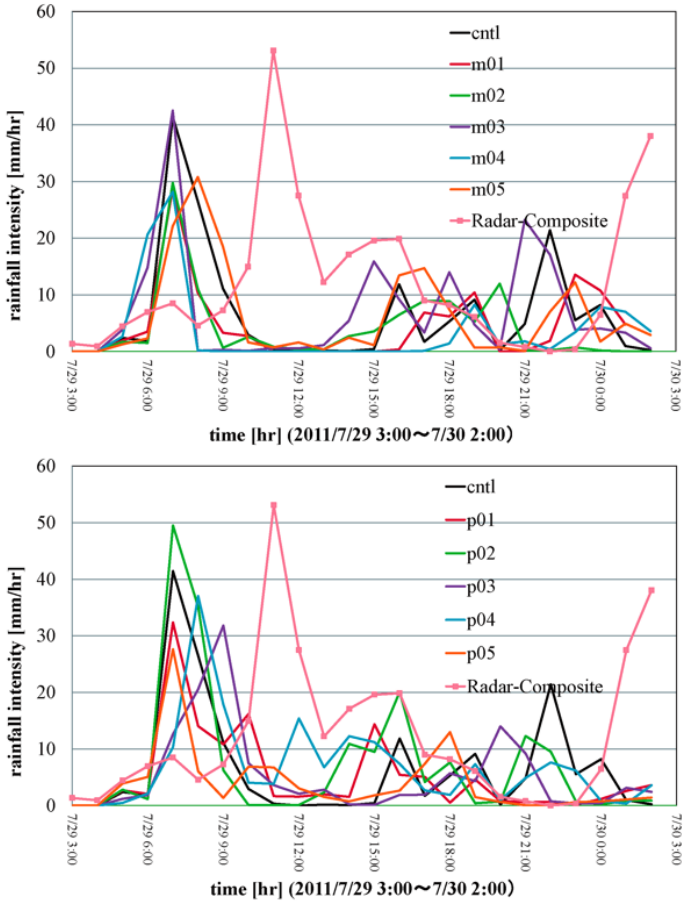

Figure 16. Catchment-averaged rainfalls with JMA-NHM 2 km-resolution ensemble simulation (upper: control run and negatively perturbed members; lower: control run and positively perturbed members).

NHESSD
3, 7411–7456, 2015

Ensemble flood forecasting to support dam water release operation

K. Kobayashi et al.

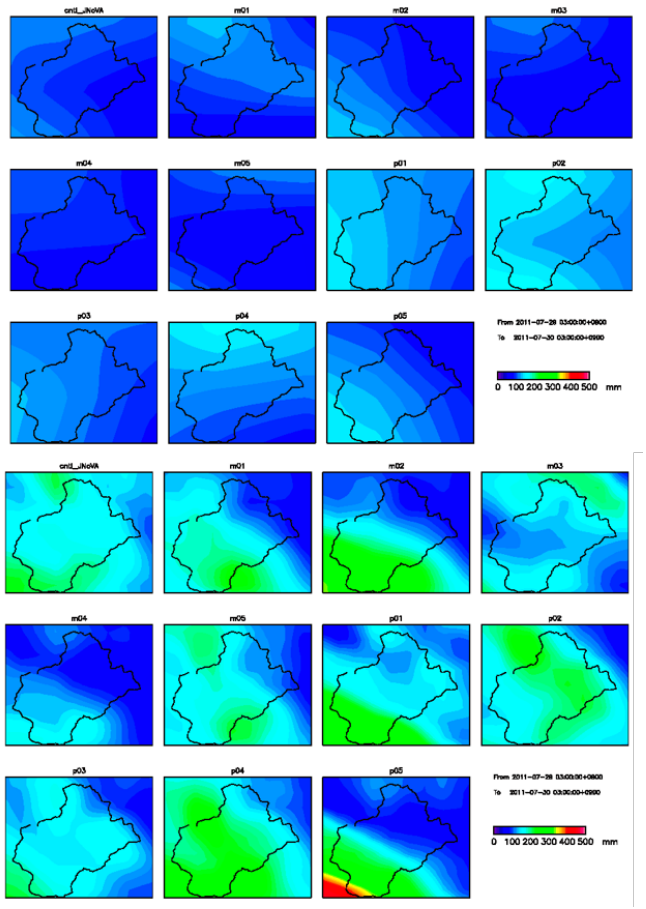

Figure 17. Spatial distributions of cumulative ensemble rainfalls (upper: 10 km resolution; lower: 2 km resolution).

NHESSD
3, 7411–7456, 2015

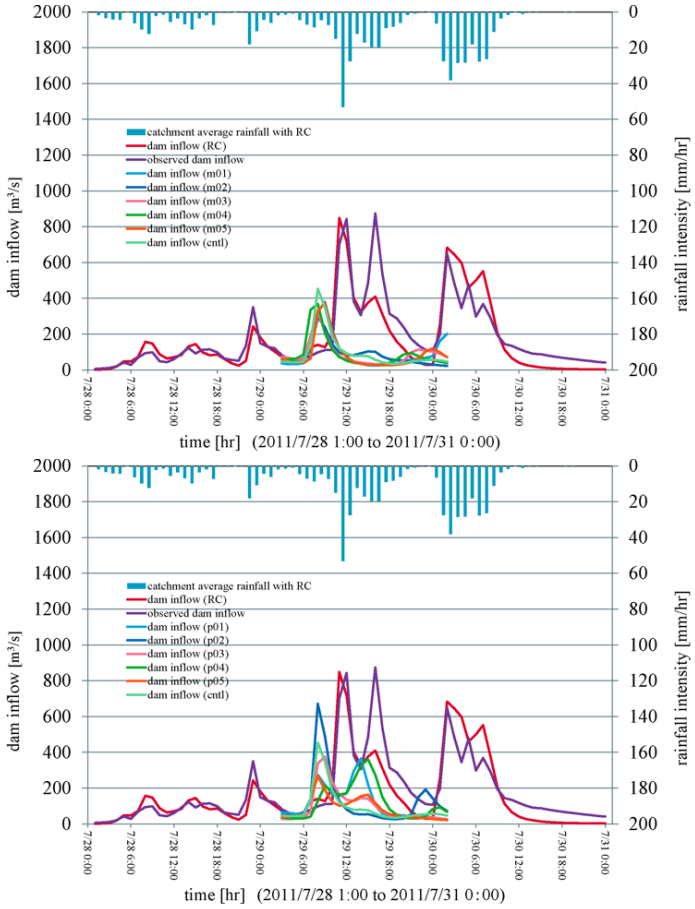

Figure 18. Results of ensemble flood simulations with 10 km resolution rainfall (upper: control run and negatively perturbed members; lower: control and positively perturbed members).

NHESSD
3, 7411–7456, 2015

Ensemble flood forecasting to support dam water release operation

K. Kobayashi et al.

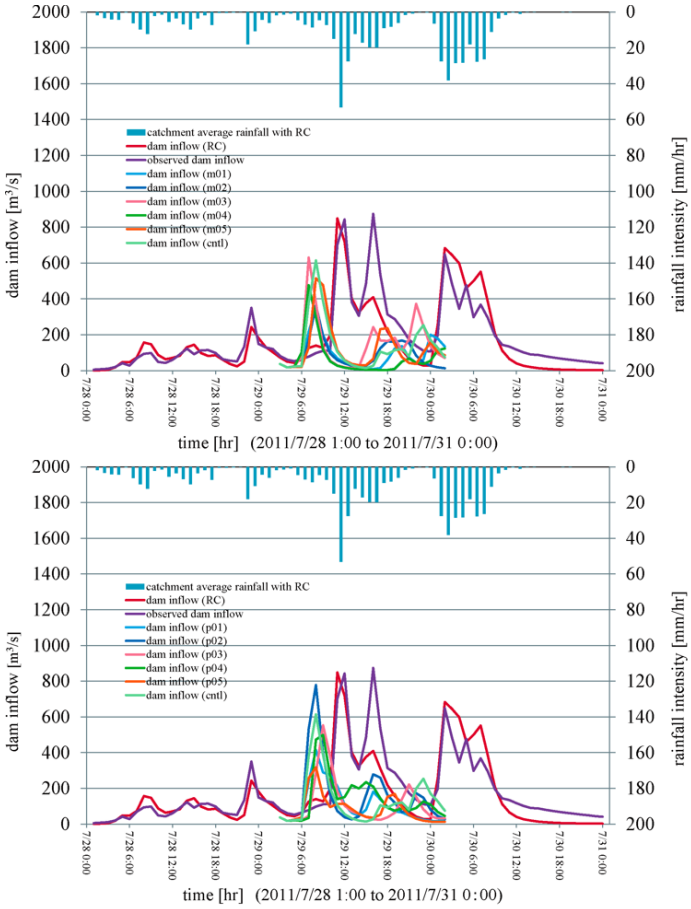

Figure 19. Results of ensemble flood simulations with 2 km resolution rainfall (upper: control run and negatively perturbed members; lower: control and positively perturbed members).

NHESSD
3, 7411–7456, 2015

Ensemble flood forecasting to support dam water release operation

K. Kobayashi et al.

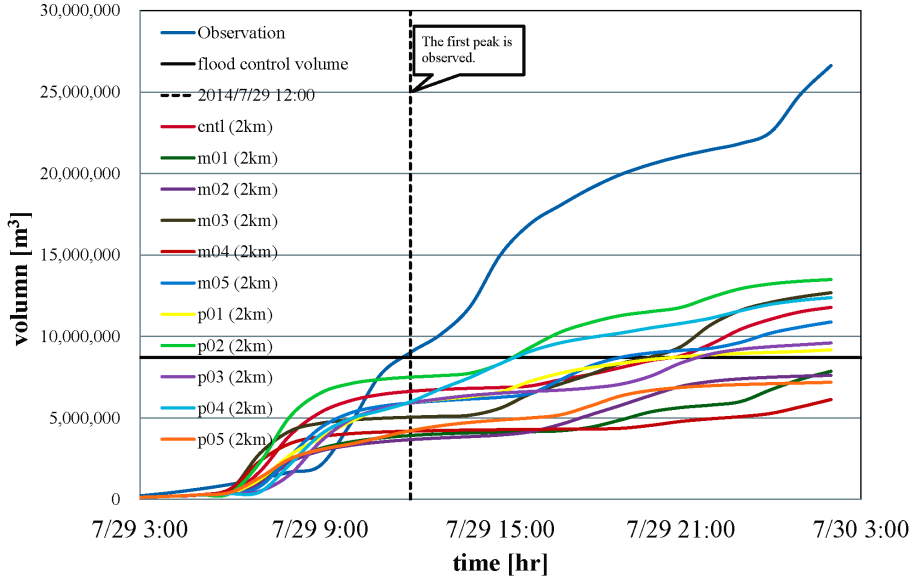

Figure 20. Inflow volume into the reservoir based on observation and 2 km ensemble simulations.

NHESSD
3, 7411–7456, 2015

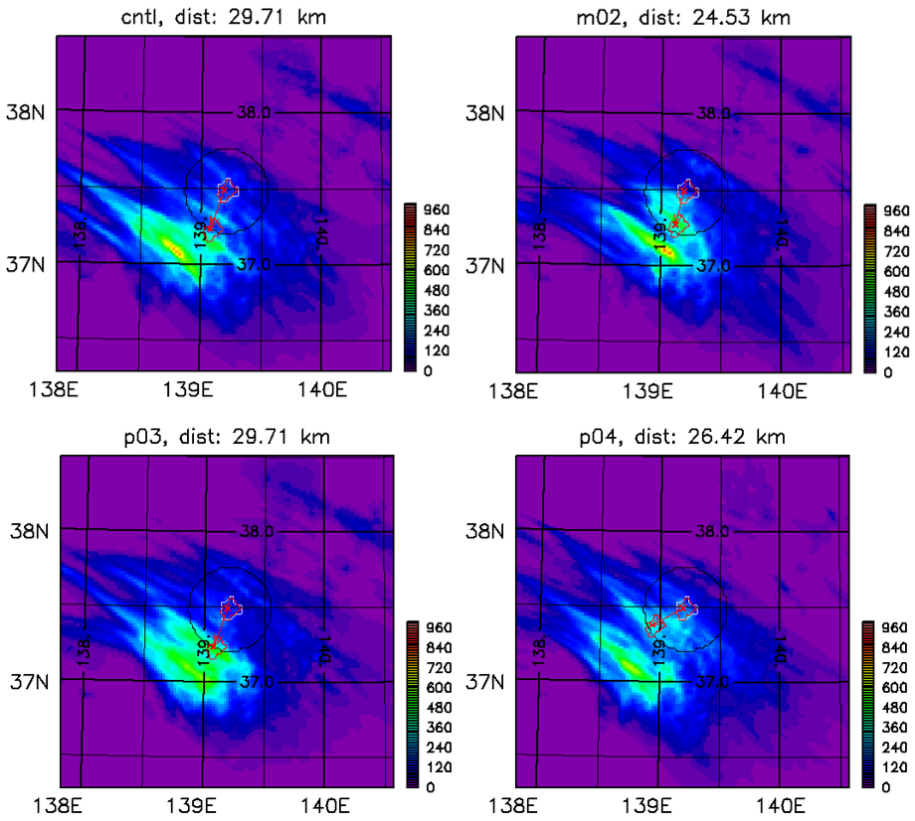

Figure 21. Examples of the position shifts of the ensemble rainfalls.

NHESSD
3, 7411–7456, 2015

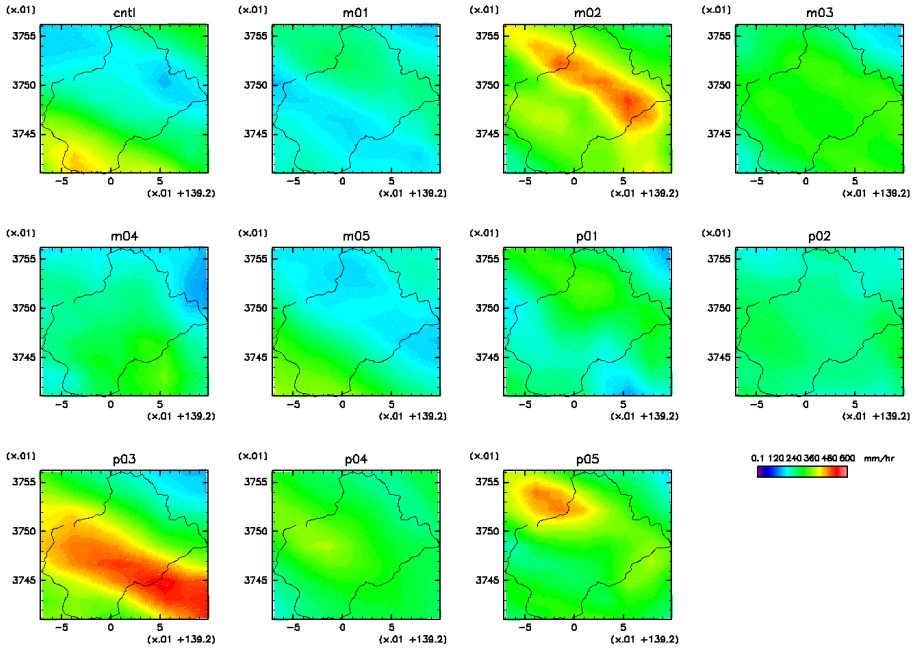

Figure 22. Spatial distributions of cumulative ensemble rainfalls with position shift (2 km resolution).

NHESSD
3, 7411–7456, 2015

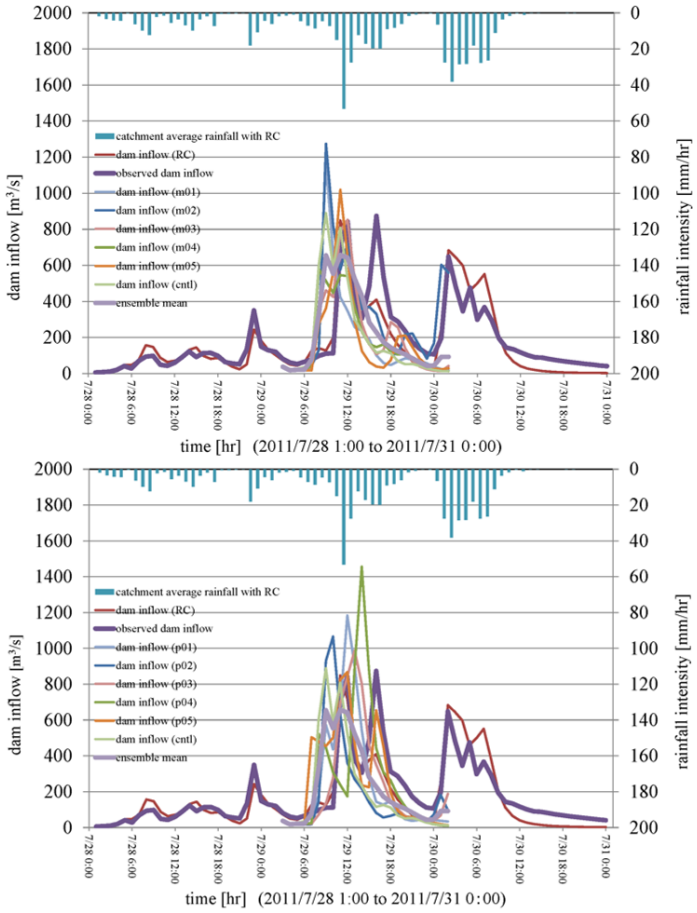

Figure 23. Results of ensemble flood simulations with rainfall position shift (upper: control run and negatively perturbed members; lower: control and positively perturbed members).

NHESSD
3, 7411–7456, 2015

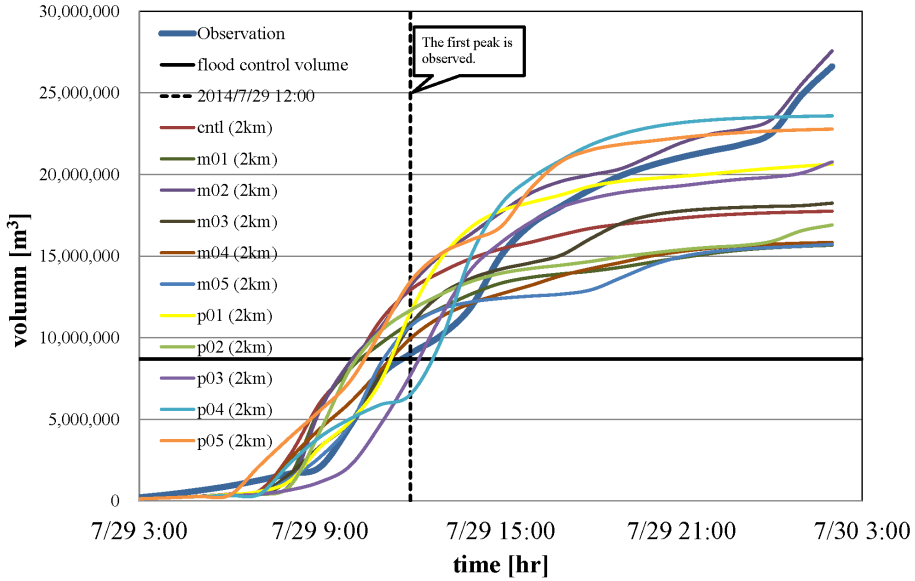

Figure 24. Inflow volume into the reservoir based on observation and ensemble simulations with rainfall position shift.

NHESSD
3, 7411–7456, 2015